 CMES, vol.99, no.5, pp.417-443, 2014

Singular Boundary Method: Three Regularization Approaches and Exterior Wave Applications

Zhuo-Jia Fu[1], Wen Chen[1,2], Jeng-Tzong Chen[3] and Wen-Zhen Qu[1]

Abstract: This study investigates the singular boundary method (SBM) with three regularization approaches for solving 2D and 3D exterior wave problems. The singular boundary method is a recent meshless boundary collocation method, which introduces the concept of source intensity factors to eliminate the singularity of the fundamental solutions. Recently, three approaches, the inverse interpolation technique (IIT), the semi-analytical technique with boundary IIT (SAT1) and the semi-analytical technique with integral mean value (SAT2), have been proposed to determine the source intensity factors for removing the singularities of Helmholtz fundamental solutions at origin. This study compares numerical accuracy and stability of these three approaches on some benchmark examples under 2D and 3D exterior wave radiation and scattering problems. Numerical investigations show that SAT1>IIT>SAT2 in numercial accuracy and SAT2>SAT1>IIT in numerical stability. Then the SBM with SAT1 is applied to water wave-structure interaction and SH wave scattering problem. For water wave-structure interaction, numerical results show that both the porosity of the cylinder sidewall and the disorder arrangement have a great effect on the free-surface elevations in the vicinity of the wave structure. For SH wave scattering by a semi-circular hill, the focusing phenomenon is revisited.

Keywords: Boundary collocation, singular boundary method, source intensity factors, singularity, Helmholtz fundamental solution, radiation and scattering.

1 Introduction

During the past decades we have witnessed a research boom on the boundary-type meshless techniques [Atluri and Zhu (2000); Chen et al. (2013)], since the con-

[1] College of Mechanics and Materials & State Key Laboratory of Hydrology-Water Resources and Hydraulic Engineering, Hohai University, Nanjing 210098, P.R. China.
[2] Corresponding author. Email: chenwen@hhu.edu.cn
[3] Department of Harbor and River Engineering, National Taiwan Ocean University, Keelung 20224, Taiwan.

struction of a mesh in the standard BEM is non trivial. They can be classified into weak and strong form categories. Among them, weak-form category includes the local boundary integral equation method [Zhu et al. (1998)], the meshless local Petrov-Galerkin method [Atluri and Zhu (1998); Zhang et al. (2013)], the boundary node method .[Mukherjee and Mukherjee (1997); Zhang et al. (2002)], the boundary face method .[Zhang et al. (2009)], the null-field boundary integral equation method [Chen et al. (2007); Lee and Chen (2013a); Lee and Chen (2013b)] and so on. Strong-form category includes the boundary point interpolation method [Gu and Liu (2002)], the method of fundamental solutions [Chen et al. (2008); Fairweather and Karageorghis (1998); Lin et al. (2011); Tsai (2008)], the boundary knot method [Chen and Tanaka (2002); Fu et al. (2011)], the boundary particle method [Fu et al. (2013); Fu et al. (2012)], the Trefftz method [Dong and Atluri (2012a); Dong and Atluri (2012b); Liu (2008)], the regularized meshless method [Chen et al. (2006); Young et al. (2005)], the modified method of fundamental solutions [Sarler (2009)], the singular boundary method [Chen (2009)] and the boundary distributed source method [Kim (2013); Liu (2010)] and so on.

This study focuses on a recent meshless boundary collocation method, the singular boundary method (SBM) [Chen (2009)], which introduces the concept of source intensity factor to regularize the singularities of fundamental solutions, in some literatures it also named as origin intensity factor. Therefore, it avoids singular numerical integrals in the boundary element method and circumvents the troublesome placement of the fictitious boundary in the method of fundamental solutions.

At first, an inverse interpolation technique (IIT) has been proposed to determine the above-mentioned source intensity factors of fundamental solutions. This SBM formulation has been successfully applied to interior and exterior Laplace [Chen and Fu (2010); Chen et al. (2009); Chen and Wang (2010)], Poisson [Wei et al. (2013)], Helmholtz [Fu and Chen (2010)] and elastostatic [Gu et al. (2011)] problems. Later, Chen and Gu [Gu et al. (2012b)] introduced the desingularization of subtracting and adding-back technique and proposed an improved singular boundary method (ISBM) for interior and exterior potential problems. Its main improvement is developing a semi-analytical technique (SAT1) to determine the source intensity factors without any inner sample nodes. The approach employs the null-field or full-field integral equations to evaluate analytically the source intensity factors on Neumann boundary conditions for Laplace equation. After that it uses the inverse interpolation technique with boundary source points to determine the source intensity factors on Dirichlet boundary conditions for Laplace equation. Then Fu and Chen used the relationships between Laplace and Helmholtz-type fundamental solutions to extend the ISBM to solve interior and exterior Helmholtz-type problems [Chen et al. (2014); Fu et al. (2014); Fu and Chen (2013)]. Recently, another semi-analytical technique (SAT2) has been proposed [Gu et al. (2012a)], whose difference with the SAT1 is implementing the integral mean value approach to determine the source intensity factors on Dirichlet boundary conditions for Laplace equation.

This study will extend the SAT2 to determine the source intensity factors of the Helmholtz fundamental solutions, and then compares numerical accuracy and stability of these three approaches (IIT, SAT1 and SAT2) on exterior wave problems. A brief outline of the paper is as follows. Section 2 describes the singular boundary method with three regularization treatments for Helmholtz problems. In Section 3, the efficiency and accuracy of these three approaches are examined in 2D and 3D benchmark examples. Section 4 presents the singular boundary method to two exterior wave scattering applications. Finally, Section 5 concludes this paper with some remarks.

2 Three regularization treatments in the SBM

The problem under consideration is the propagation of time-harmonic waves in a homogeneous isotropic medium D exterior to a closed bounded curve Γ, which is described by the Helmholtz equation

$$\nabla^2 u(x) + k^2 u(x) = 0,\ x \in D, \tag{1}$$

subjected to the boundary conditions:

$$u\,(x) = \bar{u}, \quad x \in \Gamma_D, \tag{2a}$$

$$q(x) = \frac{\partial u\,(x)}{\partial \mathbf{n}} = \bar{q}, \quad x \in \Gamma_N, \tag{2b}$$

where $k = \omega/c$ the wavenumber, ω the angular frequency, c the wave speed in the exterior medium D, and $\mathbf{n}$ the unit outward normal on physical boundary. Γ_D and Γ_N represent the essential boundary (Dirichlet) and the natural boundary (Neumann) conditions, respectively, which construct the whole closed bounded curve $\Gamma = \Gamma_D + \Gamma_N$, and u is complex-valued amplitude of radiated and/or scattered wave (velocity potential or pressure):

$$u = \begin{cases} u_R = u_T, & \text{if radiation,} \\ u_S = u_T - u_I, & \text{if scattering,} \\ u_{R+S} = u_T - u_I, & \text{if both,} \end{cases}$$

where the subscripts T, R and I denote the total, radiation and incidence wave, respectively. For the exterior wave problems, it requires guaranteeing the physical requirement that all scattered and radiated waves are outgoing. This is accomplished by imposing an appropriate radiation condition at infinity, which is termed as the Sommerfeld radiation condition:

$$\lim_{r\to\infty} r^{\frac{1}{2}(\dim-1)}\left(\frac{\partial u}{\partial r}-iku\right)=0, \tag{2c}$$

where *dim* is the problem dimension, and $i=\sqrt{-1}$. By utilizing single layer fundamental solutions, the SBM approximate solutions $u(x)$ and $q(x)$of exterior Hemholtz problem (Eqs. (1) and (2)) can be expressed as follows

$$u(x_m)=\begin{cases}\sum\limits_{j=1}^{N}\alpha_j G(x_m,s_j),\ x_m\in D\backslash\Gamma\\ \sum\limits_{j=1,j\neq m}^{N}\alpha_j G(x_m,s_j)+\alpha_m U_S^{jj},\ x_m\in\Gamma\end{cases}, \tag{3a}$$

$$q(x_m)=\frac{\partial u(x_m)}{\partial \mathbf{n}_x}=\begin{cases}\sum\limits_{j=1}^{N}\alpha_j \frac{\partial G(x_m,s_j)}{\partial \mathbf{n}_x},\ x_m\in D\backslash\Gamma\\ \sum\limits_{j=1,j\neq m}^{N}\alpha_j \frac{\partial G(x_m,s_j)}{\partial \mathbf{n}_x}+\alpha_m Q_S^{jj},\ x_m\in\Gamma\end{cases}, \tag{3b}$$

where N denotes the number of source points s_j, α_j the$j$th unknown coefficient, $\mathbf{n}_x$ the outward normal unit vector on the collocation points x_m, 2D fundamental solutions $G(x_m,s_j)=iH_0^{(1)}(kr_{mj})\Big/4$, and 3D fundamental solutions $\mathrm{G}(x_m,s_j)=e^{ikr_{mj}}\Big/(4\pi r_{mj})$, in which $H_n^{(1)}$ is the nth order Hankel function of the first kind, the Euclidean distance $r_{mj}=\left\|x_m-s_j\right\|_2$. If the collocation points and source points coincide, i.e., $x_m=s_j$, the well-known singularities are encountered. The SBM introduces the concept of the source intensity factors U_S^{jj} and Q_S^{jj} to avoid these singularities. The key issue of the SBM is how to determine these source intensity factors U_S^{jj} and Q_S^{jj}. Fortunately, it is of interest to point out that the fundamental solutions of Helmholtz equation have the similar order of the singularities as the related fundamental solutions of Laplace equation [Kirkup (1998)]. The corresponding relationships can be represented by the following asymptotic expressions

$$G(x_m,s_j)=G_0(x_m,s_j)+B,\ r_{mj}\to 0, \tag{4a}$$

$$\frac{\partial G(x_m,s_j)}{\partial \mathbf{n}_x}=\frac{\partial G_0(x_m,s_j)}{\partial \mathbf{n}_x},\ r_{mj}\to 0, \tag{4b}$$

$$\frac{\partial G(x_m,s_j)}{\partial \mathbf{n}_s}=\frac{\partial G_0(x_m,s_j)}{\partial \mathbf{n}_s},\ r_{mj}\to 0, \tag{4c}$$

where Euler constant $\gamma = 0.57721566490153286\cdots$, $\mathbf{n}_s$ the outward normal unit vector on the source points s_j, For 2D problem, Laplace fundamental solution $G_0 = -\ln(r_{mj})/(2\pi)$ and $B = -\left(\ln\left(k/2\right) + \gamma - i\pi/2\right)/(2\pi)$. For 3D problem, Laplace fundamental solution $G_0 = 1/(4\pi r_{mj})$ and $B = ik/(4\pi)$. Hence we can introduce the existing approaches to determine the source intensity factors for Laplace equation, and then implement the above-mentioned relationship to calculate the source intensity factors for Helmholtz equation. In the next section, we will introduce three approaches to determine the source intensity factors for removing the singularities of Helmholtz fundamental solutions at origin.

2.1 Inverse interpolation technique

This section will introduce a simple numerical technique, called the inverse interpolation technique (IIT) [Chen and Fu (2010); Fu and Chen (2010)], to determine the source intensity factors for Laplace equation. Then we can use the relationships between Helmholtz and Laplace fundamental solutions to determine the source intensity factors for Helmholtz equation. In the first step, the IIT requires choosing a known sample solution u_{S0} of Laplace equation and placing some sample points y_k inside the physical domain. It is noted that the sample points y_k do not coincide with the source points s_j, and the number of sample points NK should not be fewer than the source node number N on physical boundary. By using the interpolation formula (3), we can then determine the influence coefficients β_j and $\bar{\beta}_j$ by solving the following linear equations

$$\left\{G_0\left(y_k, s_j\right)\right\}\left\{\beta_j\right\} = \left\{u_{S0}\left(y_k\right)\right\}, \tag{5a}$$

$$\left\{\frac{\partial G_0\left(y_k, s_j\right)}{\partial \mathbf{n}_x}\right\}\left\{\bar{\beta}_j\right\} = \left\{\frac{\partial u_{S0}\left(y_k\right)}{\partial \mathbf{n}_x}\right\}. \tag{5b}$$

Replacing the sample point y_k with the boundary collocation point x_m, the SBM interpolation matrix (Eqs. (1) and (2)) can be written as

$$\begin{bmatrix} U_{S0}^{11} & G_0\left(x_1, s_2\right) & \cdots & G_0\left(x_1, s_N\right) \\ G_0\left(x_2, s_1\right) & U_{S0}^{22} & \cdots & G_0\left(x_2, s_N\right) \\ \vdots & \vdots & \ddots & \vdots \\ G_0\left(x_N, s_1\right) & G_0\left(x_N, s_2\right) & \cdots & U_{S0}^{NN} \end{bmatrix}\left\{\beta_j\right\} = \left\{u_{S0}\left(x_m\right)\right\} \tag{6a}$$

$$\begin{bmatrix} Q_{S0}^{11} & \frac{\partial G_0(x_1,s_2)}{\partial \mathbf{n}_x} & \cdots & \frac{\partial G_0(x_1,s_N)}{\partial \mathbf{n}_x} \\ \frac{\partial G_0(x_2,s_1)}{\partial \mathbf{n}_x} & Q_{S0}^{22} & \cdots & \frac{\partial G_0(x_2,s_N)}{\partial \mathbf{n}_x} \\ \vdots & \vdots & \ddots & \vdots \\ \frac{\partial G_0(x_N,s_1)}{\partial \mathbf{n}_x} & \frac{\partial G_0(x_N,s_2)}{\partial \mathbf{n}_x} & \cdots & Q_{S0}^{NN} \end{bmatrix}\left\{\bar{\beta}_j\right\} = \left\{\frac{\partial u_{S0}\left(x_m\right)}{\partial \mathbf{n}_x}\right\} \tag{6b}$$

The source intensity factors for Laplace equation can be calculated by:

$$U_{S0}^{mm} = \left(u_{S0}(x_m) - \sum_{j=1, s_j \neq x_m}^{N} \beta_j G_0(x_m, s_j) \right) \Bigg/ \beta_m \; x_m = s_j, x_m \in \Gamma_D \tag{7a}$$

$$Q_{S0}^{mm} = \left(\frac{\partial u_{S0}(x_m)}{\partial \mathbf{n}_x} - \sum_{j=1, s_j \neq x_m}^{N} \beta_j \frac{\partial G_0(x_m, s_j)}{\partial \mathbf{n}_x} \right) \Bigg/ \bar{\beta}_m \; x_m = s_j, x_m \in \Gamma_N \tag{7b}$$

Then the source intensity factors for the Helmholtz equation can be represented as

$$U_S^{mm} = U_{S0}^{mm} + B, \; x_m = s_j, x_m \in \Gamma_D \tag{8a}$$

$$Q_S^{mm} = Q_{S0}^{mm}, \; x_m = s_j, x_m \in \Gamma_N \tag{8b}$$

2.2 *Semi-analytical technique with boundary IIT (SAT1)*

This section will introduce a semi-analytical technique [Chen et al. (2014); Gu et al. (2012b)] to calculate the source intensity factors, it does not require the additional inner sample nodes.

2.2.1 Source intensity factors on Neumann boundary conditions

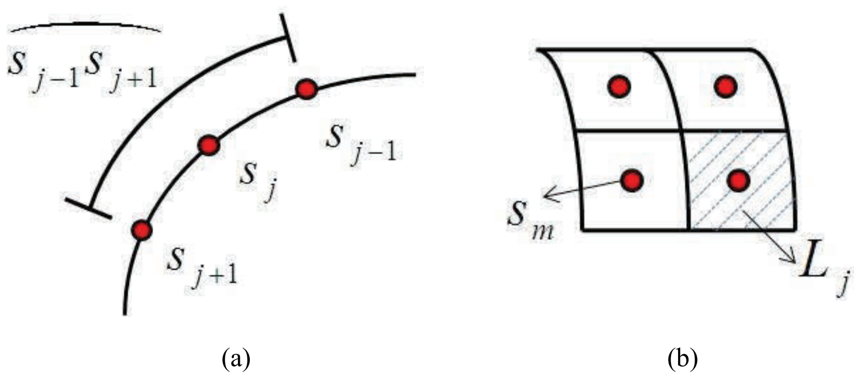

Figure 1: Schematic configuration of (a) source points s_j and the related curve on 2D problems and (b) source points s_j and the related infinitesimal area L_j on 3D problems.

By adopting the subtracting and adding-back technique in Eq. (3b) at $x_m = s_j$, we obtain

$$
\begin{aligned}
q(x_m) &= \frac{\partial u(x_m)}{\partial \mathbf{n}_x} = \sum_{j=1}^{N} \alpha_j \frac{\partial G(x_m, s_j)}{\partial \mathbf{n}_x} \\
&= \sum_{j=1}^{N} (\alpha_j - \alpha_m \Pi_{jm}) \frac{\partial G(x_m, s_j)}{\partial \mathbf{n}_x} + \alpha_m \sum_{j=1}^{N} \Pi_{jm} \left(\frac{\partial G(x_m, s_j)}{\partial \mathbf{n}_x} - \frac{\partial G_0(x_m, s_j)}{\partial \mathbf{n}_x} \right), \\
&+ \alpha_m \sum_{j=1}^{N} \Pi_{jm} \left(\frac{\partial G_0(x_m, s_j)}{\partial \mathbf{n}_x} + \frac{\partial G_0^I(x_m, s_j)}{\partial \mathbf{n}_s} \right) - \alpha_m \sum_{j=1}^{N} \Pi_{jm} \frac{\partial G_0^I(x_m, s_j)}{\partial \mathbf{n}_s}
\end{aligned}
\tag{9}
$$

where $G_0^I(x_m, s_j)$ denotes the fundamental solution of the interior Laplace equation, $\Pi_{jm} = L_j / L_m$, in which L_j is half length of the curve between source points s_{j-1} and s_{j+1} for 2D problems as shown in Fig. 1a, and L_j is the infinitesimal area of the source point s_j for 3D problems as shown in Fig. 1b. Note that $\Pi_{mm} = 1$ in both 2D and 3D problems.

According to the dependency of the outward normal vectors on the fundamental solutions of interior and exterior Laplace equations [Gu et al. (2012b); Young et al. (2005)], we have the following relationships

$$
\begin{cases}
\frac{\partial G_0(x_m, s_j)}{\partial \mathbf{n}_s} = -\frac{\partial G_0^I(x_m, s_j)}{\partial \mathbf{n}_s}, & x_m \neq s_j \\
\frac{\partial G_0(x_m, s_j)}{\partial \mathbf{n}_s} = \frac{\partial G_0^I(x_m, s_j)}{\partial \mathbf{n}_s}, & x_m = s_j
\end{cases},
\tag{10a}
$$

and

$$
\lim_{s_j \to x_m} \left(\frac{\partial G_0(x_m, s_j)}{\partial \mathbf{n}_x} + \frac{\partial G_0(x_m, s_j)}{\partial \mathbf{n}_s} \right) = 0,
\tag{10b}
$$

$$
V_m = -\frac{1}{L_m} = \sum_{j=1}^{N} \Pi_{jm} \frac{\partial G_0^I(x_m, s_j)}{\partial \mathbf{n}_s}
\tag{10c}
$$

when the boundary shape is of a straight line, Eq. (10b) is explicitly equal to zero since $\mathbf{n}_x(x_m) = \mathbf{n}_s(s_j)$ at all boundary knots. For an arbitrarily shaped smooth boundary, herein we assume that the source point s_j approaches inchmeal to the collocation point x_m along a line segment, then Eq. (10b) is tenable. Eq. (10c) can be derived based on the discretization of the reduced full-fields equations [Ochmann (1999)]. With the help of Eqs. (4) and (10), Eq. (9) can be regularized as follows

$$
q(x_m) = \sum_{j=1, j \neq m}^{N} \alpha_j \frac{\partial G(x_m, s_j)}{\partial \mathbf{n}_x} - \alpha_m \left(\sum_{j=1, j \neq m}^{N} \Pi_{jm} \frac{\partial G_0(x_m, s_j)}{\partial \mathbf{n}_s} + V_m \right).
\tag{11}
$$

By contrast with Eq. (3b) at $x_m = s_j$, we can obtain

$$Q_S^{jj} = Q_{S0}^{jj} = -V_m - \sum_{j=1, j \neq m}^{N} \Pi_{jm} \frac{\partial G_0(x_m, s_j)}{\partial \mathbf{n}_s}. \tag{12}$$

which is the source intensity factors for Neumann boundary conditions in Eq. (3b).

2.2.2 *Source intensity factors on Dirichlet boundary conditions*

Next the source intensity factors U_{S0}^{jj} can be calculated by the inverse interpolation technique [Chen et al. (2014); Gu et al. (2012b)]. This strategy chooses a sample solution $\bar{u}_0$ of Laplace equation, e.g. $\bar{u}_0 = x + y + c$ for 2D problems and $\bar{u}_0 = x + y + z + c$ for 3D problems. Then $2N+1$ linear equations are obtained with $2N+1$ unknowns (U_0^{jj}, β_j, c) on N boundary source points and one inner point x_I.

$$\bar{u}_0(x_m) = \sum_{j=1, j \neq m}^{N} \beta_j G_0(x_m, s_j) + \beta_m U_0^{jj} + c, \; x_m = s_j, \tag{13a}$$

$$\frac{\partial \bar{u}_0(x_m)}{\partial \mathbf{n}_x} = \sum_{j=1, j \neq m}^{N} \beta_j \frac{\partial G_0(x_m, s_j)}{\partial \mathbf{n}_x} + \beta_m Q_0^{jj}, \; x_m = s_j, \tag{13b}$$

$$\bar{u}_0(x_I) = \sum_{j=1}^{N} \beta_j G_0(x_I, s_j) + c, \; x_I \neq s_j. \tag{13c}$$

Therefore, the source intensity factors U_S^{jj} in Eq. (3a) can now be determined indirectly by calculating the source intensity factors U_{S0}^{jj} of Laplace equation by using the expression (8a).

2.3 Semi-analytical technique with integral mean value (SAT2)

This section will introduce a recently developed semi-analytical technique [Gu et al. (2012a)], which do not require the inverse interpolation technique. As with Section 2.2.1, the regularized SBM formulation for the Neumann boundary condition (3b) can be expressed as follows

$$q(x_m) = \sum_{j=1, j \neq m}^{N} \alpha_j \frac{\partial G(x_m, s_j)}{\partial \mathbf{n}_x} - \alpha_m \left(\sum_{j=1, j \neq m}^{N} \Pi_{jm} \frac{\partial G_0(x_m, s_j)}{\partial \mathbf{n}_s} + V_m \right). \tag{14}$$

and

$$Q_S^{jj} = Q_{S0}^{jj} = -V_m - \sum_{j=1, j \neq m}^{N} \Pi_{jm} \frac{\partial G_0(x_m, s_j)}{\partial \mathbf{n}_s}. \tag{15}$$

is the aforementioned source intensity factors for the Neumann boundary condition. Next the regularized expression for the Dirichlet boundary equation (3a) can be performed using the strategy proposed in the reference [Sarler (2009)], where the corresponding source intensity factors are directly set as an average value of the Laplace fundamental solution over a line segments. This can be formulated as

$$U_{S0}^{jj} = \frac{1}{L_m}\int_{\Gamma_s} G(x_m, s_j)d\Gamma_s = -\frac{1}{2\pi L_m}\int_{\Gamma_s} \ln\left\|x_m - s_j\right\|_2 d\Gamma_s, \qquad (16a)$$
$$x_m = s_j, \quad \text{for 2D problems.}$$

$$U_{S0}^{jj} = \frac{1}{L_m}\int_{\Gamma_s} G(x_m, s_j)d\Gamma_s = \frac{1}{4\pi L_m}\int_{\Gamma_s} \frac{1}{\left\|x_m - s_j\right\|_2} d\Gamma_s, \qquad (16b)$$
$$x_m = s_j, \quad \text{for 3D problems.}$$

Then the source intensity factors U_S^{jj} for the Dirichlet boundary condition can be calculated by using the expression (8a).

3 Numerical investigations and discussions

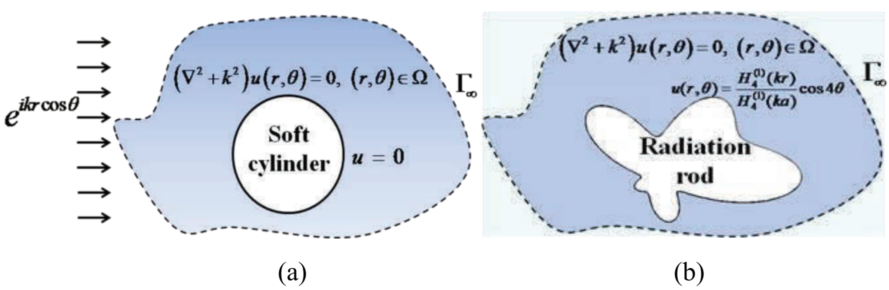

Figure 2: Sketch of (a) the scattering problem for an infinite soft cylinder and (b) the radiation problem of an infinite irregular-shaped rod.

In this section, the efficiency, accuracy and convergence of the above-mentioned three treatments (IIT, SAT1 and SAT2) in the SBM are implemented to solve 2D and 3D exterior wave problems. The numerical accuracy is calculated by the relative root mean square errors (RMSE) *Lerr(u)* which is defined as

$$Lerr(u) = \sqrt{\frac{1}{NT}\sum_{k=1}^{NT}\left|u(k) - \bar{u}(k)\right|^2} \Bigg/ \sqrt{\frac{1}{NT}\sum_{k=1}^{NT}\left|\bar{u}(k)\right|^2}, \qquad (17)$$

where $\bar{u}(k)$ and $u(k)$ are the analytical and numerical solutions at x_i, respectively, and NT is the total number of test points in the domain of interest. Unless otherwise specified, in all the following numerical cases, the inner sample nodes y_k are uniform angular distribution on the same boundary shape of physical geometry with scaling factor $\left(1-2/L_k\right)$ for the IIT and the inner point x_I=(0.5,0.5) for the SAT1 in 2D problems, and the inner sample nodes y_k are uniform angular distribution on the same boundary shape of physical geometry with scaling factor $\left(1-2/\sqrt{L_k}\right)$ for the IIT and the inner point x_I=(0.5,0.5,0.5) for the SAT1 in 3D problems.

Example 1: Scattering problem of a soft infinite circular cylinder (Dirichlet boundary condition)

We consider a plane wave $e^{ikr\cos\theta}$ scattered by a soft infinite circular cylinder as shown in Fig. 2a. The analytical solution of the scattering field u_S [Chen et al. (2007)] is

$$u_S(r,\theta) = -\frac{J_0(ka)}{H_0^{(1)}(ka)}H_0^{(1)}(kr) \; -2\sum_{n=1}^{\infty} i^n \frac{J_n(ka)}{H_n^{(1)}(ka)}H_n^{(1)}(kr)\cos n\theta. \tag{18}$$

Fig. 3 shows the error analysis of the SBM with three treatments for 2D scattering problem with $ka = 40$. The analytical solutions in this case are calculated by using the first 100 terms in the above series representation (18). The test points (*NT=101*) are uniform angular distribution on the circle with radius 1.2. It can be found that all of these three methods converge with the increasing boundary node number N. In this case, the SBM with SAT1 provides better results than the SBM with IIT and SAT2 under the same number of boundary knots, the slope of the convergence curve is about -3. The SBM with SAT2 has the slowest convergence rate and the slope of the convergence curve is about -1. While the SBM with IIT has the same convergence rate to the SAT1 with modestly increasing boundary node number (N=10000), but it converges slowly with further increasing boundary node number. This may result from the non-optimal source intensity factors calculated by the IIT.

Consider the radiation problem of an infinite soft irregular-shaped rod as shown in Fig. 2b. The analytical solution of the radiation field u_R is

$$u_R(r,\theta) = \frac{H_4^{(1)}(kr)}{H_4^{(1)}(ka)}\cos 4\theta. \tag{19}$$

Fig. 4 shows the error analysis of the SBM with three treatments for 2D radiation problem of a soft infinite irregular-shaped rod with $ka = 1$. The test points (*NT=101*) are uniform angular distribution on the circle with radius $1.5/0.425$. Similar to the conclusion in Example 1, the SBM with SAT1 has the best performance among these three treatments, the SBM with SAT2 converges very slowly.

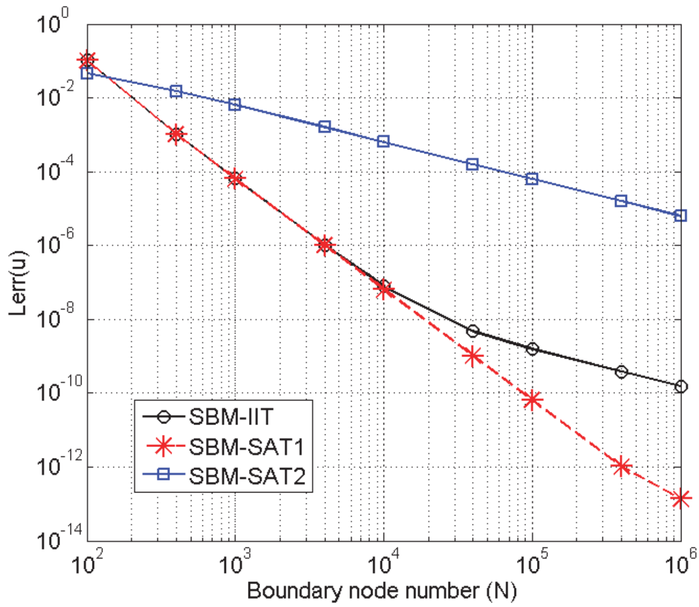

Figure 3: Convergence analysis *Lerr(u)* of the SBM with IIT, SAT1 and SAT2 for the scattering problem of a soft infinite cylinder with $ka = 40$

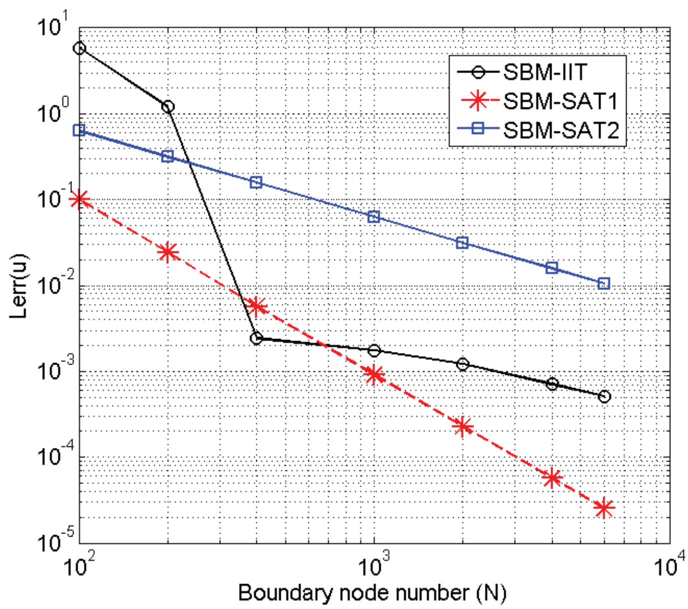

Figure 4: Convergence analysis *Lerr(u)* of the SBM with IIT, SAT1 and SAT2 for the radiation problem of an soft infinite irregular-shaped rod with $ka = 1$.

Numerical stability is very sensitive to the placement of sample nodes in the SBM with IIT.

Example 3: Scattering problem of a soft sphere (Dirichlet boundary condition)

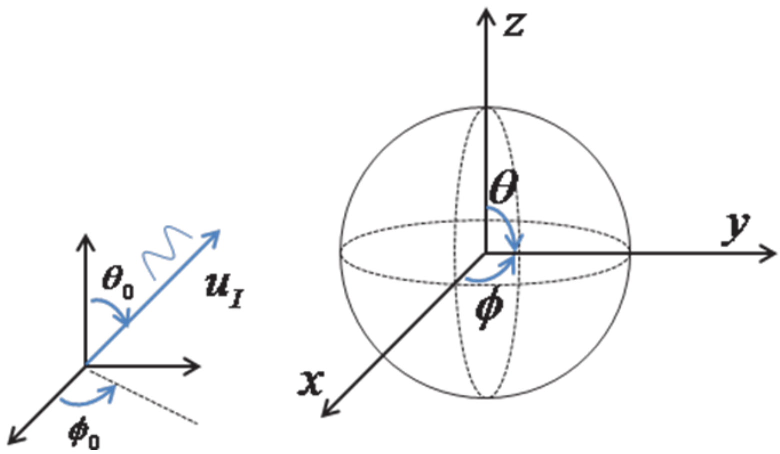

Figure 5: Sketch of a soft spherical scatterer with the incident wave u_I.

Consider the scattering problem of a soft sphere with the incident plane wave $u_I = e^{ik(z\cos\theta_0+\sin\theta_0(x\cos\varphi_0+y\sin\varphi_0))}$, where (θ_0,φ_0) denotes the angle of the incident plane wave in the spherical coordinates as shown in Fig. 5. The analytical solution of the scattering field u_S [Chen et al. (2010)] is

$$u(r,\theta,\varphi) = j_0(ka)\frac{h_0^{(1)}(kr)}{h_0^{(1)}(ka)} + \sum_{m=1}^{\infty} i^m(2m+1)\, j_m(ka)\frac{h_m^{(1)}(kr)}{h_m^{(1)}(ka)} + \sum_{m=1}^{\infty}\sum_{v=1}^{m} \frac{2i^m(2m+1)(m-v)!}{(m+v)!} j_m(ka)\frac{h_m^{(1)}(kr)}{h_m^{(1)}(ka)} P_m^v(\cos\theta_0)\, P_m^v(\cos\theta)\cos(v(\varphi-\varphi_0)) \tag{20}$$

Fig. 6 shows the error analysis of the SBM with three treatments for 3D scattering problem with $ka = 1$. The analytical solutions in this case are calculated by using the first 30 terms in the above series representation (20). The test points (*NT=100*) are uniform angular distribution on the surface of the sphere with radius 1.25. It can be found that all of these three methods converge with the increasing boundary node number N. In this case, the SBM with SAT1 provides better results than the SBM with IIT and SAT2 under the same number of boundary knots, the slope of the convergence curve is about -1.5. The SBM with SAT2 has the slowest convergence rate and the slope of the convergence curve is about -0.5. While the SBM with IIT

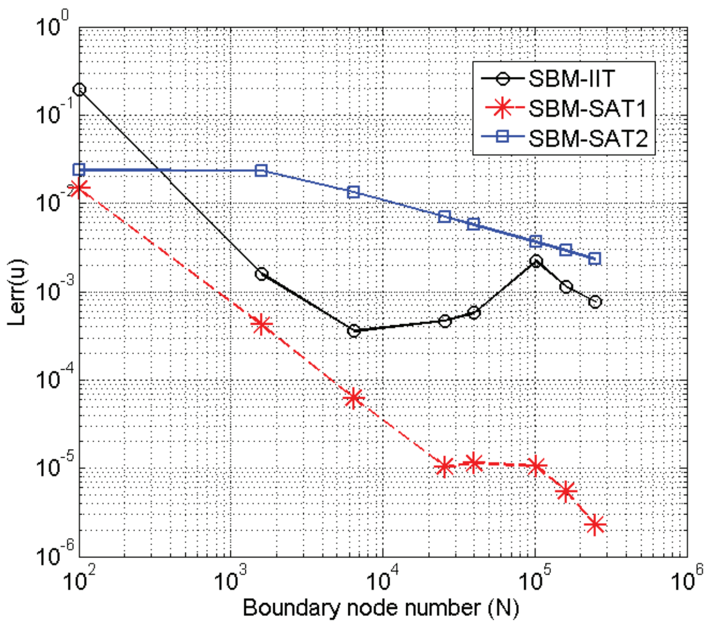

Figure 6: Convergence analysis *Lerr(u)* of the SBM with IIT, SAT1 and SAT2 for the scattering problem of an soft sphere with $ka = 1$.

has the same convergence rate to the SAT1 with modestly increasing boundary node number (*N*=10000), but it converges slowly with further increasing boundary node number. This may result from the non-optimal source intensity factors calculated by the IIT.

Example 4: Radiation model for a soft ellipsoid (Dirichlet boundary condition)

Consider the radiation problem of a soft ellipsoid $\left\{(x,y,z)|x^2+y^2+\frac{z^2}{9}\le 1\right\}$ as shown in Fig. 7. The analytical solution of the radiation field u_R is

$$u_R(r,\theta,\varphi) = \frac{e^{ikr}}{r}. \tag{21}$$

Fig. 8 shows the error analysis of the SBM with three treatments for 3D radiation problem of a soft ellipsoid with $ka = 1$. The test points (*NT=100*) are uniform angular distribution on the surface of the ellipsoid $\left\{(x,y,z)|x^2+y^2+\frac{z^2}{9}\le 1.25^2\right\}$. Similar to the conclusion in Example 3, the SBM with SAT1 has the best performance among these three treatments, the SBM with SAT2 converges very slowly. Numerical accuracy has a heavy oscillation with further increasing boundary node number (N>10000) by using the SBM with IIT.

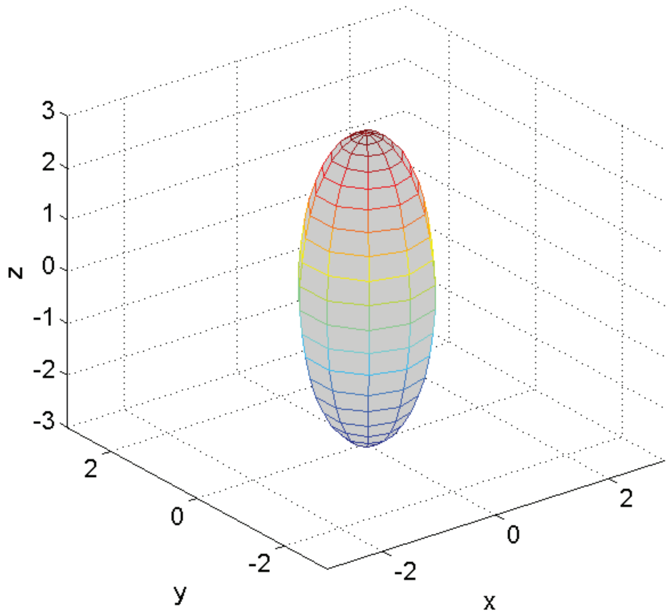

Figure 7: Sketch of the radiation problem of a soft ellipsoid.

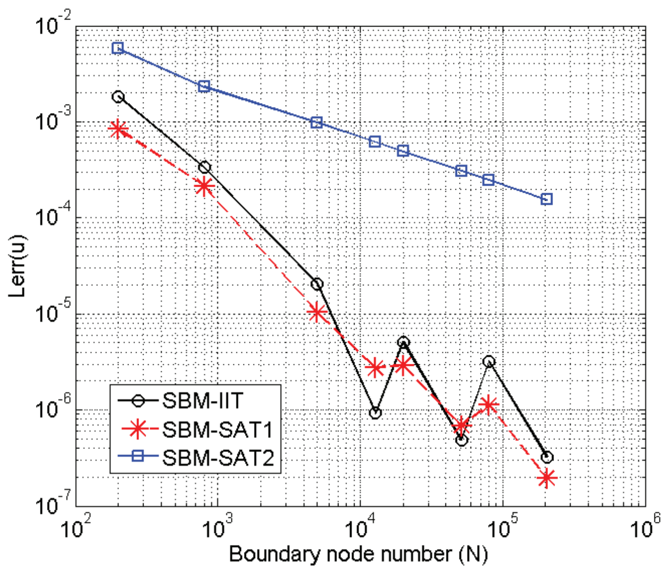

Figure 8: Convergence analysis *Lerr(u)* of the SBM with IIT, SAT1 and SAT2 for the radiation problem of an soft ellipsoid with $ka = 1$.

Generally speaking, the above-mentioned numerical results show that SAT1 > IIT> SAT2 in numercial accuracy and SAT2>SAT1>IIT in numerical stability for solving 2D and 3D exterior wave radiation and scattering problems.

4 Exterior wave scattering applications

In this section, the SBM with SAT1 is implemented to two exterior wave scattering applications. First we consider water wave scattering problem. Under the assumptions of the potential flow and linear wave theory, 3D water wave-structure interaction problem shown in Fig.9a can be reduced to 2D water wave scattering problem shown in Fig. 9b by removing the depth dependence [Chen et al. (2011b); Chen et al. (2012); Evans and Porter (1997)]. Then the mathematical model can be represented as

$$\left(\Delta+k^2\right)\varphi^j(x_1,x_2)=0,\ (x_1,x_2)\in\Omega_j, j=0,1,2,\cdots,n, \tag{22}$$

$$\frac{\partial\varphi^0}{\partial\mathbf{r}_j}=-\frac{\partial\varphi^j}{\partial\mathbf{r}_j},\ (x_1,x_2)\in\partial\Omega_j, j=1,2,\cdots,n, \tag{23}$$

$$\frac{\partial\varphi^j}{\partial\mathbf{r}_j}=-\mathrm{i}kG_p\left(\varphi^j-\varphi^0\right),\ (x_1,x_2)\in\partial\Omega_j, j=1,2,\cdots,n, \tag{24}$$

$$\lim_{r\to\infty} r^{\frac{1}{2}}\left(\frac{\partial\left(\varphi^0-\varphi_I\right)}{\partial r}-ik\left(\varphi^0-\varphi_I\right)\right)=0,\ (x_1,x_2)\in\Omega_0, \tag{25}$$

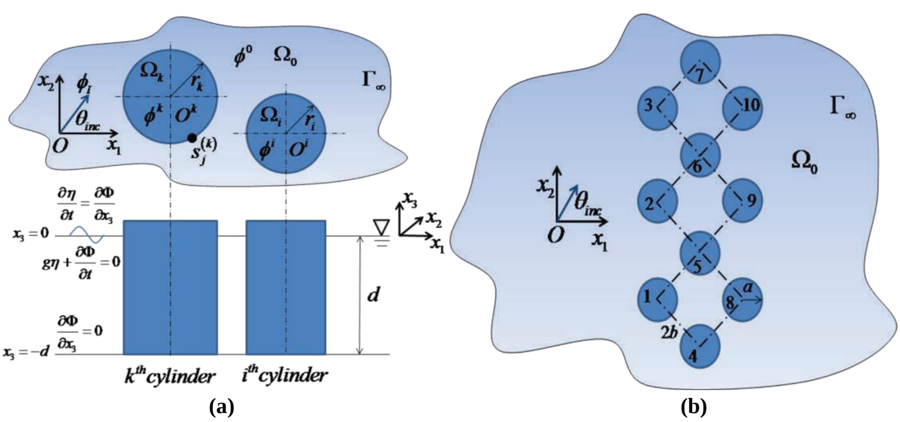

Figure 9: Problem statement of (a) 3D water wave-structure interaction and (b) the related 2D water wave problem.

where $\mathbf{r}_j$ denotes the unit normal vector on the jth cylinder surface, $\varphi_I(x_1,x_2) = e^{ik(x_1\cos\theta_{inc}+x_2\sin\theta_{inc})}$ is the incident water wave and its amplitude is A, $|\eta| = |A\varphi(x_1,x_2)|$ the free-surface elevation, and the wavenumber k is the real root of the dispersion relationship $\omega^2 = gk\tanh kd$, ω the angular frequency, g the gravitational acceleration, d the water depth and $i = \sqrt{-1}$. G_p=$\gamma\rho\omega/(\mu k)$ the dimensionless porosity [Chen et al. (2011b)], in which μ the dynamic viscosity coefficient, γ a material constant having the dimension of length and ρ the fluid density. G_p=0 means the impermeable cylinder. The entire plane potential-field region R^2 is divided into n+1 sub-regions, n finite circular regions $\Omega_j = \left\{(x_1,x_2)\,|\,\left(x_1 - x_1^j\right)^2 + \left(x_2 - x_2^j\right)^2 \le r_j^2\right\}, j = 1,2,\cdots,n$ and an infinite region $\Omega_0 = \Omega^e$, where $O^j = \left(x_1^j, x_2^j\right)$ represents the coordinate of the center of the jth circular cylinder and r_j is the radius of the related cylinder. Therefore, $\varphi^j(x_1,x_2)$ denotes the horizontal velocity potential in the sub-region Ω_j, and $\varphi^0 = \varphi_I + \sum_{j=1}^{n} \varphi_S^{(j)}$, where $\varphi_S^{(j)}$ is the horizontal velocity potential of the scattering wave by the jth circular cylinder.

In the SBM simulation, we set some parameters as $a = 0.4$, $b = 0.5$, $d = 2$, $\theta_{inc} = 0$, $ka = 4.08482$, and place 100 boundary nodes on the boundary of each cylinder. Fig. 10 shows the free-surface elevation in the vicinity of ten-cylinder array with different dimensionless porosity (G_p=$0, 0.0001, 1$) and different disorder parameters (τ=$0, 0.1$). As shown in Fig. 11, the disorder displacement of each cylinder center away from its original regular position can be calculated by $\Delta x_j = \gamma_j(b-a)\tau\cos(2\pi\gamma_j), \Delta y_j = \gamma_j(b-a)\tau\sin(2\pi\gamma_j)$, where the random number γ_j can be generated by using Matlab function "rand".

From Fig. 10a, it can be observed that the near-trapped mode phenomenon [Chen et al. (2011b); Evans and Porter (1997)] is revisited in the wave structure with impermeable regular cylinders (G_p=0, τ=0), and the maximum amplitude appearing on the inner sides of the cylinders is about 150 times over the incident wave amplitude. Numerical results demonstrate that both the porosity of the cylinder sidewall and the disorder arrangement have a great effect on the free-surface elevations in the vicinity of the wave structure. We can see from Fig. 10 that the increase of the porosity leads to the decrease of the maximum free-surface amplitude, and small disorder arrangement can also reduce the maximum free-surface amplitude remarkably. When the porosity parameter is relatively large (G_p=1), the porosity of the structure has more influence to avoid the occurrence of near-trapped mode phenomenon than the disorder arrangement of the structure. When the porosity parameter is relatively small (G_p=0.0001), the disorder arrangement of the structure has more influence to avoid the occurrence of near-trapped mode phenomenon than the porosity of the structure.

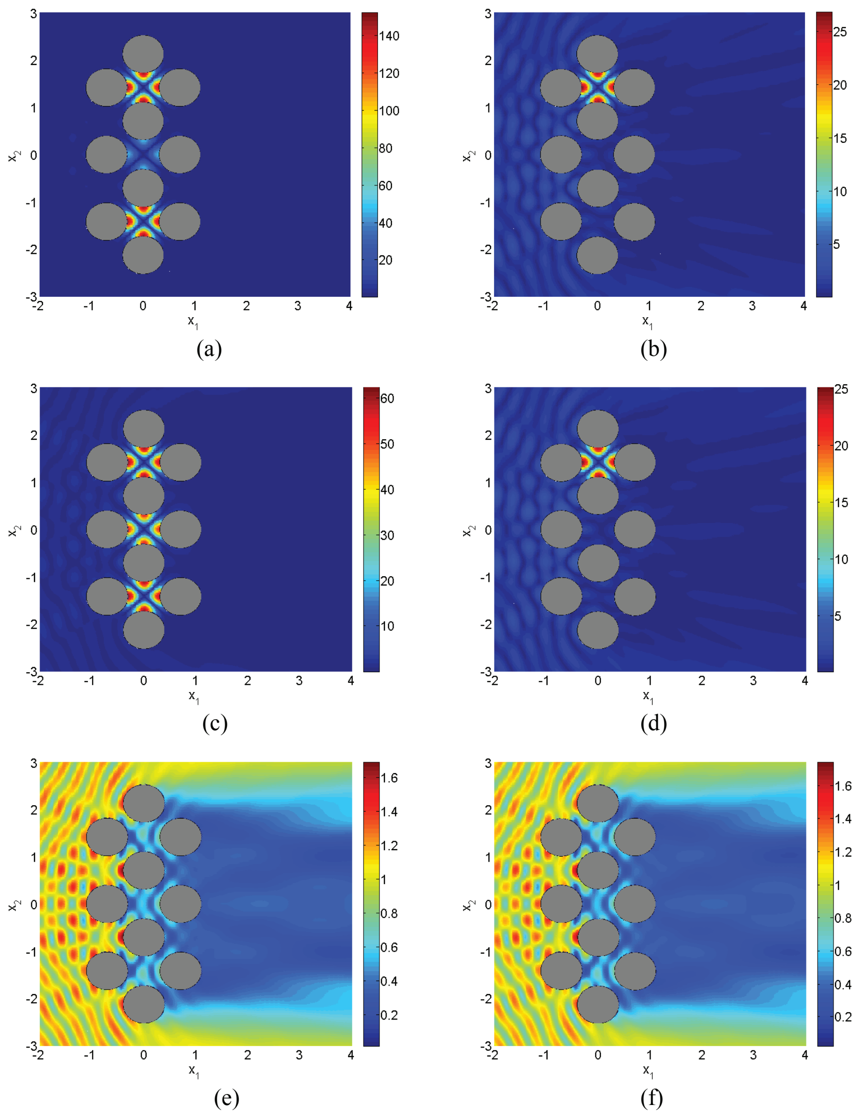

Figure 10: SBM results of the free-surface elevation in the vicinity of ten-cylinder array with different porosity and disorder parameters: (a)G_p=0,τ=0; (b)G_p=0,τ=0.1; (c) G_p=0.0001,τ=0; (d) G_p=0.0001,τ=0.1; (e) G_p=1,τ=0; (f) G_p=1,τ=0.1.

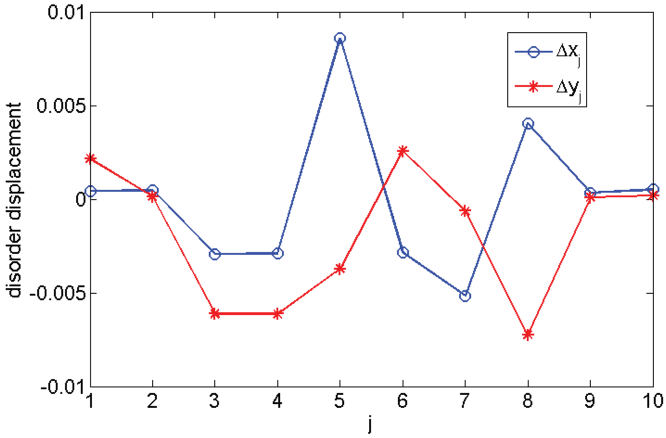

Figure 11: Disorder displacement $(\Delta x_j, \Delta y_j)$ of jth cylinder center with disorder parameter τ=0.1.

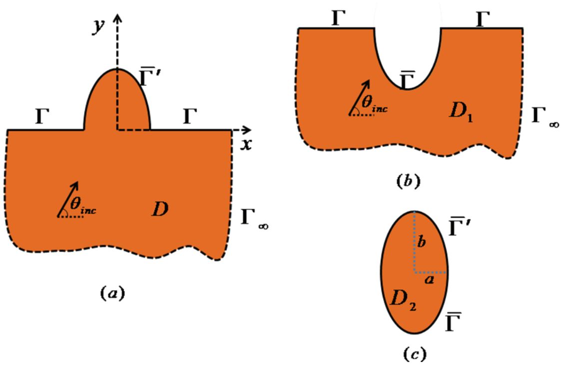

Figure 12: Decomposition and conjunction technique for SH wave scattering problem. (a) Original region D, (b) a semi-infinite region D_1 and (c) an interior region D_2.

Then SH wave scattering problem with a semi-circular hill ($a = b = 1$) is considered [Tsaur and Chang (2009)] as shown in Fig. 12. $\varphi_I(x_1, x_2) = e^{ik(x_1 \cos\theta_{inc} + x_2 \sin\theta_{inc})}$ is incident SH wave expression, where θ_{inc} is the incident wave angle, k denote the wavenumber. For easy comparison with the other reference results, the dimensionless frequency η is defined as $\eta = \frac{ka}{\pi}$. The mathematical model of SH wave scattering problem is

$$\begin{cases} \left(\Delta+k^2\right)u\left(x,y\right)=0,\ \left(x,y\right)\in D \\ t\left(x,y\right)=\mu\frac{\partial u(x,y)}{\partial \mathbf{n}}=0,\ \left(x,y\right)\in\Gamma\cup\bar{\Gamma}' \\ \lim\limits_{r\to\infty}r^{\frac{1}{2}}\left(\frac{\partial(u-u_{inc})}{\partial r}-ik\left(u-u_{inc}\right)\right)=0,\ \left(x,y\right)\in\Gamma_\infty \end{cases} \tag{26}$$

By implementing decomposition and conjunction technique [Yuan and Liao (1996)], the mathematical model can be represented as

$$\begin{cases} \left(\Delta+k^2\right)u_1\left(x,y\right)=0,\ \left(x,y\right)\in D_1 \\ t_1\left(x,y\right)=\mu\frac{\partial u_1(x,y)}{\partial \mathbf{n}}=0,\ \left(x,y\right)\in\Gamma \\ \lim\limits_{r\to\infty}r^{\frac{1}{2}}\left(\frac{\partial(u_1-u_{inc})}{\partial r}-ik\left(u_1-u_{inc}\right)\right)=0,\ \left(x,y\right)\in\Gamma_\infty \end{cases}, \tag{27}$$

and

$$\begin{cases} \left(\Delta+k^2\right)u_2\left(x,y\right)=0,\ \left(x,y\right)\in D_2 \\ t_2\left(x,y\right)=\mu\frac{\partial u_2(x,y)}{\partial \mathbf{n}}=0,\ \left(x,y\right)\in\bar{\Gamma}' \end{cases}, \tag{28}$$

with the continuity condition on fictitious boundary $\bar{\Gamma}$

$$\begin{cases} u_1\left(x,y\right)=u_2\left(x,y\right),\ \left(x,y\right)\in\bar{\Gamma} \\ t_1\left(x,y\right)=-t_2\left(x,y\right),\ \left(x,y\right)\in\bar{\Gamma} \end{cases}. \tag{29}$$

For the interior problem, we choose $\bar{G}\left(x_m,s_j\right)=-Y_0\left(kr_{mj}\right)/4$ as the basis function, where Y_0 is zero-order Bessel functions of the second kind. The related source intensity factors can be calculated by Eq. (8) with $B=-\left(\ln\left(k/2\right)+\gamma\right)/(2\pi)$. In the SBM simulation, we place 100 boundary nodes on the boundary $\bar{\Gamma}\cup\bar{\Gamma}'$ and 50 auxiliary nodes on the boundary Γ.

Fig. 13 shows the surface displacement amplitude versus x with different incident wave angles and different dimensionless frequencies ($\theta_{inc}=\frac{\pi}{2}$,$\eta=2$; $\theta_{inc}=\frac{\pi}{6}$, $\eta=3$). From Fig. 13, one can find that the present SBM performs well with the reference results [Chen et al. (2011a); Tsaur and Chang (2009)].

Then the focusing phenomenon of vertical SH wave scattering ($\theta_{inc}=\frac{\pi}{2}$) by a semi-circular hill is revisited. Fig. 14 plots the spectral variation of surface displacement amplitudes along the central axis of the semi-circular hill, ranging from the top of the hill (y=1) to the bottom of the fictitious boundary $\bar{\Gamma}$ (y=-1) with the dimensionless frequency η from 0 to 12. It should be mentioned that the present SBM results are in good accordance with the reference results [Tsaur and Chang (2009)]. From Fig. 14, it can be observed that the focusing of wave energy mostly occurs at the depth between y=0.5 and 0.75. However, the maximum surface displacement amplitudes may take place on the top of the semi-circular hill (y=1) at some frequencies (η=5.0-5.3 and 8.5-9.5).

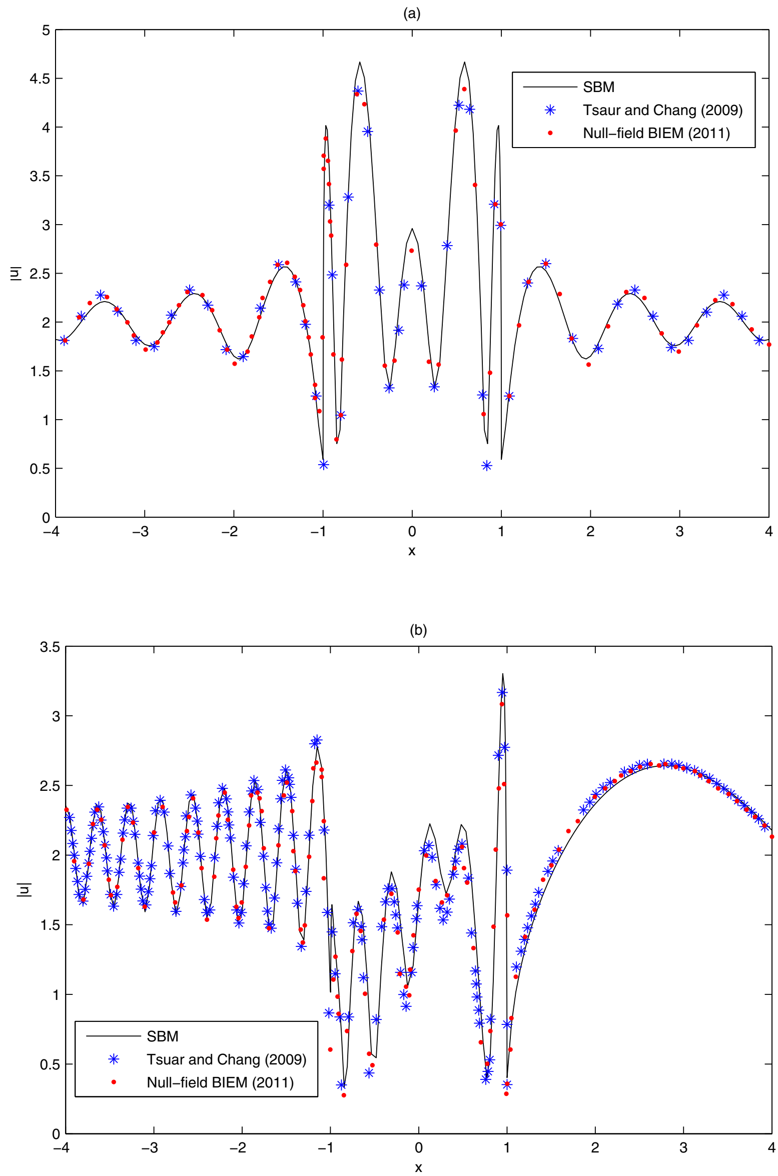

Figure 13: Surface displacement amplitudes $|u|$ versus x with (a) incident wave angle $\theta_{inc} = \frac{\pi}{2}$ and the dimensionless frequency $\eta = 2$; (b) $\theta_{inc} = \frac{\pi}{6}$ and $\eta = 3$.

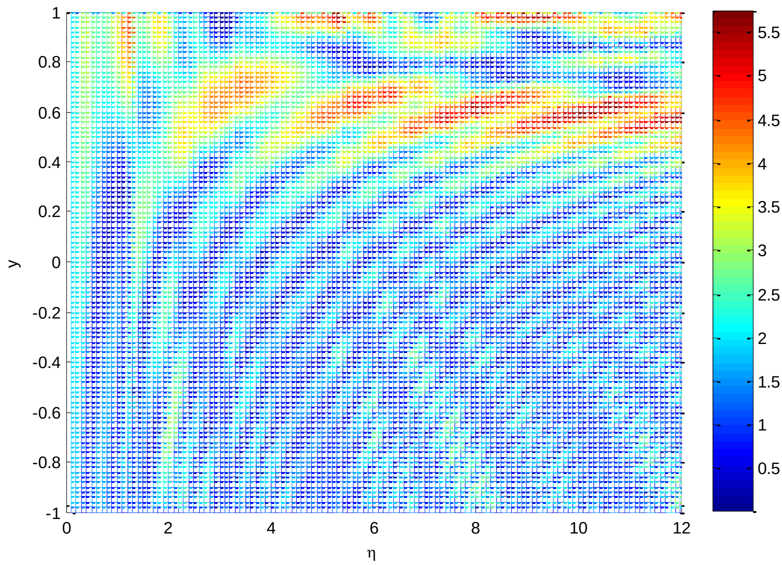

Figure 14: Spectral variation of displacement amplitudes $|u|$ along the central axis of the semi-circular hill for the incident SH wave angle of $\theta_{inc} = \frac{\pi}{2}$

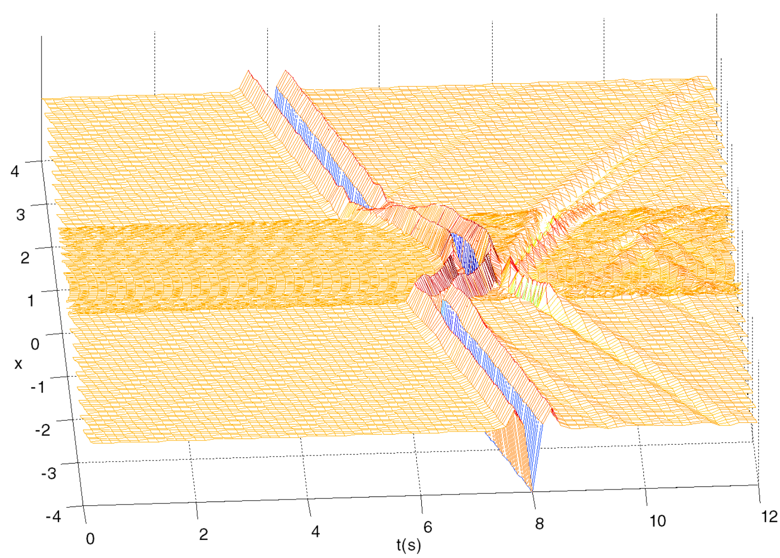

Figure 15: Synthetic seismograms of SH wave scattering by a semi-circular hill with the incident wave angle of $\theta_{inc} = \frac{\pi}{3}$.

$$u(t) = \left(2\pi^2 f_c^2 t^2 - 1\right) e^{-\pi^2 f_c^2 t^2} \tag{30}$$

where f_c denotes the characteristic frequency of Ricker wavelet. In the SBM simulation, we set f_c=1.5Hz and compute the surface displacement amplitudes $|u|$ with 96 dimensionless frequencies (η=0.0625$(N_f - 1)$, N_f=1,2,$\cdots$,96) as the frequency-domain solutions, and then introduce the Fast Fourier Transform to obtain the time-domain synthetic seismic response from the frequency-domain solutions. Fig. 15 displays the synthetic seismograms of SH wave scattering by a semi-circular hill with the incident wave angle $\theta_{inc} = \frac{\pi}{3}$. The present SBM results are in good agreement with the reference results [Tsaur and Chang (2009)].

5 Conclusions

This study makes the numerical comparison on three treatments for calculating the source intensity factors in the singular boundary method. Numerical results shows that the SBM with SAT1 provides the best performance among these three methods, the SBM with SAT2 converges very slowly. By employing the SBM with IIT, numerical stability is very sensitive to the placement of sample nodes. In this study, we propose a strategy to select the appropriate sample nodes, however, this strategy still needs further verification and improvement. Generally speaking, numerical investigations show that SAT1>IIT>SAT2 in numercial accuracy and SAT2>SAT1>IIT in numerical stability for solving 2D and 3D exterior wave radiation and scattering problems.

Then the SBM with SAT1 is implemented to two exterior wave applications. Numerical results demonstrate that the present SBM results are in good agreement with the reference results. For water wave-structure interaction, numerical investigations show that both the porosity of the cylinder sidewall and the disorder arrangement have a great effect on the free-surface elevations in the vicinity of the wave structure. For SH wave scattering by a semi-circular hill, the focusing phenomenon is revisited, and the related synthetic seismograms are plotted by introducing the Fast Fourier Transform. Further study is to introduce fast matrix algorithms [Bebendorf and Rjasanow (2003); Liu (2009); Yan et al. (2010)] to accelerate the SBM simulation for large-scale exterior wave applications.

Acknowledgement: The work described in this paper was supported by the National Basic Research Program of China (973 Project No. 2010CB832702), the National Science Funds for Distinguished Young Scholars of China (Grant No.11125208), the National Science Funds of China (Grant No. 11302069, 11372097), the Fundamental Research Funds for the Central Universities (Grant No. 2013B32814) and the 111 Project (Grant No. B12032).

References

Atluri, S. N.; Zhu, T. (1998): A new Meshless Local Petrov-Galerkin (MLPG) approach in computational mechanics. *Computational Mechanics*, vol. 22, no. 2, pp. 117-127.

Atluri, S. N.; Zhu, T. (2000): New concepts in meshless methods. *International Journal for Numerical Methods in Engineering*, vol. 47, no. 1-3, pp. 537-556.

Bebendorf, M.; Rjasanow, S. (2003): Adaptive Low-Rank Approximation of Collocation Matrices. *Computing*, vol. 70, no. 1, pp. 1-24.

Chen, C. S.; Karageorghis, A.; Smyrlis, Y. S. (2008): *The Method of Fundamental Solutions – A Meshless Method*. Dynamic Publishers.

Chen, J. T.; Chen, C. T.; Chen, P. Y.; Chen, I. L. (2007): A semi-analytical approach for radiation and scattering problems with circular boundaries. *Computer Methods in Applied Mechanics and Engineering*, vol. 196, no. 25-28, pp. 2751-2764.

Chen, J. T.; Lee, J. W.; Wu, C. F.; Chen, I. L. (2011a): SH-wave diffraction by a semi-circular hill revisited: A null-field boundary integral equation method using degenerate kernels. *Soil Dynamics and Earthquake Engineering*, vol. 31, no. 5-6, pp. 729-736.

Chen, J. T.; Lee, Y. T.; Lin, Y. J. (2010): Analysis of multiple-spheres radiation and scattering problems by using a null-field integral equation approach. *Applied Acoustics*, vol. 71, pp. 690-700.

Chen, J. T.; Lin, Y. J.; Lee, Y. T.; Wu, C. F. (2011b): Water wave interaction with surface-piercing porous cylinders using the null-field integral equations. *Ocean Engineering*, vol. 38, no. 2-3, pp. 409-418.

Chen, J. T.; Wu, C. F.; Chen, I. L.; Lee, J. W. (2012): On near-trapped modes and fictitious frequencies for water wave problems containing an array of circular cylinders using a null-field boundary integral equation. *European Journal of Mechanics - B/Fluids*, vol. 32, pp. 32-44.

Chen, K. H.; Chen, J. T.; Kao, J. H. (2006): Regularized meshless method for solving acoustic eigenproblem with multiply-connected domain. *CMES: Computer Modeling in Engineering & Sciences*, vol. 16, no. 1, pp. 27-39.

Chen, W. (2009): Singular boundary method: A novel, simple, meshfree, boundary collocation numerical method. (in Chinese). *Acta Mechanica Solida Sinica*, vol. 30, no. 6, pp. 592-599.

Chen, W.; Fu, Z.; Chen, C. S. (2013): *Recent Advances on Radial Basis Function Collocation Methods*. Springer Berlin.

Chen, W.; Fu, Z. J. (2010): A novel numerical method for infinite domain potential problems. *Chinese Science Bulletin*, vol. 55, vol. 16, pp. 1598-1603.

Chen, W.; Fu, Z. J.; Wei, X. (2009): Potential Problems by Singular Boundary Method Satisfying Moment Condition. *Cmes-Computer Modeling in Engineering & Sciences*, vol. 54, no. 1, pp. 65-85.

Chen, W.; Tanaka, M. (2002): A meshless, integration-free, and boundary-only RBF technique. *Computers & Mathematics with Applications*, vol. 43, no. 3-5, pp. 379-391.

Chen, W.; Wang, F. Z. (2010): A method of fundamental solutions without fictitious boundary. *Engineering Analysis with Boundary Elements*, vol. 34, no. 5, pp. 530-532.

Chen, W.; Zhang, J. Y.; Fu, Z. J. (2014): Singular boundary method for modified Helmholtz equations. *Engineering Analysis with Boundary Elements*, vol. 44, pp. 112-119.

Dong, L.; Atluri, S. N. (2012a): Development of 3 D Trefftz Voronoi Cells with Ellipsoidal Voids &/or Elastic/Rigid Inclusions for Micromechanical Modeling of Heterogeneous Materials. *CMC: Computers Materials and Continua*, vol. 30, no. 1, pp. 39.

Dong, L.; Atluri, S. N. (2012b): A Simple Multi-Source-Point Trefftz Method for Solving Direct/Inverse SHM Problems of Plane Elasticity in Arbitrary Multiply-Connected Domains. *CMES:Computer Modeling in Engineering & Sciences*, vol. 85, no. 1, pp. 1-43.

Evans, D. V.; Porter, R. (1997): Near-trapping of waves by circular arrays of vertical cylinders. *Applied Ocean Research*, vol. 19, no. 2, pp. 83-99.

Fairweather, G.; Karageorghis, A. (1998): The method of fundamental solutions for elliptic boundary value problems. *Advances in Computational Mathematics*, vol. 9, no. 1-2, pp. 69-95.

Fu, Z. J.; Chen, W.; Gu, Y. (2014): Burton-Miller-type singular boundary method for acoustic radiation and scattering. *Journal of Sound and Vibration*, vol. 333, no. 16, pp. 3776-3793.

Fu, Z. J.; Chen, W.; Yang, H. T. (2013): Boundary particle method for Laplace transformed time fractional diffusion equations. *Journal of Computational Physics*, vol. 235, pp. 52-66.

Fu, Z. J.; Chen, W. A novel boundary meshless method for radiation and scattering problems. *Advances in Boundary Element Techniques XI*, Berlin, Germany, pp. 83-

90.

Fu, Z. J.; Chen, W. Water wave interaction with multiple surface-piercing porous cylinders by singular boundary method. *11TH INTERNATIONAL CONFERENCE OF NUMERICAL ANALYSIS AND APPLIED MATHEMATICS 2013: ICNAAM 2013*, pp. 928-931.

Fu, Z. J.; Chen, W.; Qin, Q. H. (2011): Boundary knot method for heat conduction in nonlinear functionally graded material. *Engineering Analysis with Boundary Elements*, vol. 35, no. 5, pp. 729-734.

Fu, Z. J.; Chen, W.; Zhang, C. Z. (2012): Boundary particle method for Cauchy inhomogeneous potential problems. *Inverse Problems in Science and Engineering*, vol. 20, no. 2, pp. 189-207.

Gu, Y.; Chen, W.; He, X. Q. (2012a): Domain-decomposition singular boundary method for stress analysis in multi-layered elastic materials. *CMC: Computers Materials & Continua*, vol. 29, no. 2, pp. 129-154.

Gu, Y.; Chen, W.; Zhang, C. Z. (2011): Singular boundary method for solving plane strain elastostatic problems. *International Journal of Solids and Structures*, vol. 48, no. 32, pp. 2549-2556.

Gu, Y.; Chen, W.; Zhang, J. (2012b): Investigation on near-boundary solutions by singular boundary method. *Engineering Analysis with Boundary Elements*, vol. 36, no. 8, pp. 1173-1182.

Gu, Y. T.; Liu, G. R. (2002): A boundary point interpolation method for stress analysis of solids. *Computational Mechanics*, vol. 28, no. 1, pp. 47-54.

Kim, S. (2013): An improved boundary distributed source method for two-dimensional Laplace equations. *Engineering Analysis with Boundary Elements*, vol. 37, no. 7, pp. 997-1003.

Kirkup, S. (1998): *The boundary element method in acoustics*. Integrated Sound Software.

Lee, J. W; Chen, J. T. (2013a): A Semianalytical Approach for a Nonconfocal Suspended Strip in an Elliptical Waveguide. *Microwave Theory and Techniques, IEEE Transactions on*, vol. 60, no. 12, pp. 3642-3655.

Lee, Y. T.; Chen, J. T. (2013b): Null-field approach for the antiplane problem with elliptical holes and/or inclusions. *Composites Part B: Engineering*, vol. 44, no. 1, pp. 283-294.

Lin, J.; Chen, W.; Wang, F. (2011): A new investigation into regularization techniques for the method of fundamental solutions. *Mathematics and Computers in Simulation*, vol. 81, no. 6, pp. 1144-1152.

Liu, C. S. (2008): A highly accurate MCTM for inverse Cauchy problems of

Laplace equation in arbitrary plane domains. *CMES-Computer Modeling in Engineering & Sciences*, vol. 35, pp. 91-111.

Liu, Y. J. (2009): *Fast Multipole Boundary Element Method-Theory and Applications in Engineering*. Cambridge University Press, Cambridge.

Liu, Y. J. (2010): A new boundary meshfree method with distributed sources. *Engineering Analysis with Boundary Elements*, vol. 34, no. 11, pp. 914-919.

Mukherjee, Y. X.; Mukherjee, S. (1997): The boundary node method for potential problems. *International Journal for Numerical Methods in Engineering*, vol. 40, no. 5, pp. 797-815.

Ochmann, M. (1999): The full-field equations for acoustic radiation and scattering. *The Journal of the Acoustical Society of America*, vol. 105, no. 5, pp. 2574-2584.

Sarler, B. (2009): Solution of potential flow problems by the modified method of fundamental solutions: Formulations with the single layer and the double layer fundamental solutions. *Engineering Analysis with Boundary Elements*,vol. 33, no. 12, pp. 1374-1382.

Tsai, C. C. (2008): The method of fundamental solutions with dual reciprocity for thin plates on Winkler foundations with arbitrary loadings. *Journal of Mechanics*, vol. 24, no. 2, pp. 163-171.

Tsaur, D. H.; Chang, K. H. (2009): Scattering and focusing of SH waves by a convex circular-arc topography. *Geophysical Journal International*, vol. 177, no. 1, pp. 222-234.

Wei, X.; Chen, W.; Fu, Z. J. (2013): Solving inhomogeneous problems by singular boundary method. *Journal of Marine Science and Technology-Taiwan*, vol. 21, no. 1, pp. 8-14.

Yan, Z. Y.; Zhang, J.; Ye, W.; Yu, T. X. (2010): Numerical characterization of porous solids and performance evaluation of theoretical models via the precorrected-FFT accelerated BEM. *CMES: Computer Modeling in Engineering & Sciences*, vol. 55, no. 1, pp. 33.

Young, D. L.; Chen, K. H.; Lee, C. W. (2005): Novel meshless method for solving the potential problems with arbitrary domain. *Journal of Computational Physics*, vol. 209, no. 1, pp. 290-321.

Yuan, X.; Liao, Z. P. (1996): Surface motion of a cylindrical hill of circular-arc cross-section for incident plane SH waves. *Soil Dynamics and Earthquake Engineering*, vol. 15, no. 3, pp. 189-199.

Zhang, J.; Qin, X.; Han, X.; Li, G. (2009): A boundary face method for potential problems in three dimensions. *International Journal for Numerical Methods in*

Engineering, vol. 80, no. 3, pp. 320-337.

Zhang, J.; Yao, Z.; Li, H. (2002): A hybrid boundary node method. *International Journal for Numerical Methods in Engineering*, vol. 53, no. 4, pp. 751-763.

Zhang, T.; Dong, L.; Alotaibi, A.; Atluri, S. N. (2013): Application of the MLPG Mixed Collocation Method for Solving Inverse Problems of Linear Isotropic/Anisotropic Elasticity with Simply/Multiply-Connected Domains. *CMES:Computer Modeling in Engineering & Sciences*, vol. 94, no. 1, pp. 1-28.

Zhu, T.; Zhang, J. D; Atluri, S. N. (1998): A local boundary integral equation (LBIE) method in computational mechanics, and a meshless discretization approach. *Computational Mechanics*, vol. 21, no. 3, pp. 223-235.